The template effect of a SiF_6^{2-} guest drives the formation of a heteroleptic Fe(II) coordination helicate

Nuria Capó,[a] Leoní A. Barrios,*[,a] Joan Cardona,[a] Jordi Ribas-Ariño,[b] Simon J. Teat,[c] Olivier Roubeau[d] and Guillem Aromí*[,a]

The anion SiF_6^{2-} exerts a strong template effect, driving the assembly of two different bispiridylpyrazolyl ligands into a triple stranded Fe(II) dinuclear heteroleptic helicate, engendering a new class within the large family of cordination helicates.

Supramolecular metallo-helicates of the type $[M_xL_y]^m$ (m = 0 or +n) are an important class of coordination assemblies.[1-4] They arise from the confluence of the geometric requirements of their two essential components, metal ions and multi-topic ligands, through a self-recognition process. The latter can be perceived as the realization of an interactional algorithm following the processing of molecular information.[5] The most common are triple[6-9] and double[10-13] stranded dinuclear helicates, $[M_2L_2]^m$ and $[M_2L_3]^m$, usually arising from tetra- and six-coordinate metals, respectively, together with bis-bidentate ligands.[14] Quadruple stranded helicates, $[M_2L_4]^m$, are less common and necessitate metals with high coordination numbers.[15, 16] Ligands with three or more chelating sites have produced helicates with more than two metallic nodes, $[M_xL_y]^m$ (x > 2).[4, 17-19] Very often, the internal cavity within dinuclear helicates is occupied by a guest. The cavity-guest volume relationship is crucial, but other conditions for a good fit are the symmetry or electronic properties of both, the guest and the capsule. In the host, these are mainly controlled by the strands of the helicate. On the other hand, one can find cationic,[20, 21] neutral[22] or anionic[23, 24] guests. This multipartite nature allows introducing molecular functions *via* the different components. Thus, *i*) the metals may introduce single-molecule magnet (SMM) behavior,[25] spin crossover (SCO)[26, 27] or luminescent properties,[28] *ii*) the strands may bring properties such as fluorescence[6] or photo-isomerization ability,[29] and *iii*) the guest may be exploited to introduce optical properties[22] or differential guest-exchange properties.[30] This provides an entry into multifunctional systems, ideally producing synergic effects.[31] We have been exploiting *bis*-pyrazolylpyridine type ligands such as L1, L2 or L3 (Fig. 1) because predictably, they react with Fe(II) to produce $[Fe_2L_3]^{4+}$ helicates exhibiting SCO behaviour. The volume of the central cavity is tuneable through the choice of the spacer between coordinating pockets, while the pyrazolyls' N–H groups point inside this space, facilitating H-bond interactions with suitable guests. With ligand L1, halide ion guests, X^-, are trapped (X= Cl, Br). The nature of X determines the SCO temperature of the $(X@[Fe_2(L1)_3])^{3+}$ helical assembly both, in the solid state[32] and in solution.[33] Ligands L2 and L3, with a longer spacer, allow the incorporation of a bigger guest. Specifically, a $[Cr(ox)_3]^{-3}$ (ox^{-2}=oxalate) coordination complex that acts an SMM has been located inside a SCO $[Fe_2L_2]^{+4}$ host.[34] Arguably, only suitable guests, G, allow the formation of the $G@[Fe_2L_3]^h$ species (h, charge of the ensemble), as determined by size, symmetry and chemical nature of both, guest and cavity.

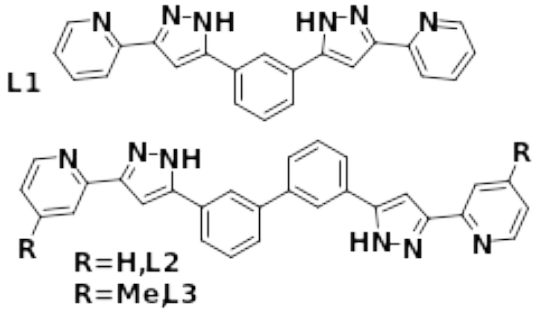

Figure 1. Ligands 1,3-bis-(1-(pyridine-2-yl)-pyrazol-3-yl)-benzene (L1), 3,3′-bis(3-(pyridin-2-yl)-1H-pyrazol-5-yl)-1,1′-biphenyl (L2) and 3,3′-bis(3-(4-picolin-2-yl)-1H-pyrazol-5-yl)-1,1′-biphenyl (L3).

We have discovered here the selective formation of heteroleptic $[Fe_2(L1)(L')_2]^{+4}$ (L' = L2, **1**; L3, **2**) helicates, driven by the template effect of an SiF_6^{2-} guest, that perfectly accommodates inside the cavity of this specific ligand combination. On the contrary, the guest ClO_4^- does not have the symmetry to facilitate this assembly, thus favoring the exclusive formation of the new homoleptic helicates $(ClO_4@[Fe_2(L')_3])^{3+}$ (L' = L2, **3**; L3, **4**), also reported here.

Mixing in MeOH L1 and L2 together with $Fe(BF_4)_2$ and excess Bu_4NPF_6 furnishes a homogeneous crystalline phase, following the diffusion of Et_2O into the resulting red solution. Single crystal X-ray diffraction (SCXRD) data unveiled the composition of this phase as $SiF_6@[Fe(L1)(L2)_2](PF_6)_2$ (**1**, see details in the SI). The inclusion of SiF_6^{2-} was unexpected, since silicon was not part of any reagent. It originates from the transfer of BF_4^- fluoride ions to the silica (SiO_2) glass of the tubes. *In situ* F^- formation[36] from decomposition of BF_4^- has been previously observed to generate SiF_6^{2-} from glass.[37] Here, bulk generation of SiF_6^{2-} from glass and BF_4^- may be driven by the strong template effect leading to **1**. The presence of side products arising from aerial oxidation of Fe(II) to Fe(III) was avoided by performing the reaction in inert atmosphere. The derivative $SiF_6@[Fe(L1)(L2)_2](BF_4)_2$ (**1a**) was then prepared under stoichiometric conditions, using the precursors $Fe(BF_4)_2$ and $(Bu_4N)_2SiF_6$ according to the reaction depicted in eq. 1, in a polypropylene container. In this case, the inert atmosphere is not necessary presumably, because the ready availability of the guest accelerates the main reaction.

$(Bu_4N)_2SiF_6 + 2Fe(BF_4)_2 + L1 + 2\ L2 \rightarrow$

$\rightarrow SiF_6@[Fe(L1)(L2)_2](BF_4)_2 + 2Bu_4NPF_6$ (1)

The template effect is replicated if the related new ligand L3 (Fig. 1) is used instead of L2. This change was intended to influence the magnetic properties of the assembly. L3 was prepared *via* the Claisen condensation of diacetylbiphenyl with the ester 4-methylpyridine-2-carboxylate to obtain a *bis*-β-

diketone that was then converted to the corresponding *bis*-pyrazolylpyridine with hydrazine (See SI). The procedures to obtain **1** were carried out using L3 (with both, glass or $(Bu_4N)_2SiF_6$ as source of silicon), yielding crystals of SiF_6@[Fe(L1)(L3)$_2$]$(PF_6)_2$ (**2**) and SiF_6@[Fe(L1)(L3)$_2$]$(BF_4)_2$ (**2a**), respectively, suitable for SCXRD.

The asymmetric unit of **1** contains one $(SiF_6$@[Fe(L1)(L2)$_2$]$)^{2+}$ supramolecular assembly (Fig. 2, S1 and S2) and two PF_6^- cations that ensure electroneutrality, in addition of crystallization solvents. The main component is a triple stranded helicate made of one L1 and two L2 ligands that chelate and keep two pseudo-octahedral Fe(II) centers 10.170 Å apart. The ligands' conformations generate a cavity perfectly suited to accommodate a SiF_6^{2-} guest, fixed by six strong [F···H–N] hydrogen bonds (Table S3). The combination of ligands keeps the guest's center of gravity separated from the Fe···Fe axis (Fig. S2), as gauged by a Fe–Si–Fe angle of 152.84°. Both enantiomers of the helicate are present in the racemic unit cell. At 100 K, the average Fe–N bond distances are 2.18 and 2.14 Å for Fe1 and Fe2, respectively, indicating that, the first ion lies in the high-spin (HS) state, while a portion of the Fe2 centres exhibits low spin (LS). The structure of **1a** (Fig. S3) is very similar to that of **1**, with BF_4^- counter-ions instead of PF_6^- (see all structural details in the SI). This causes both ions to exhibit distinctly different spin states, with average Fe–N distances of 2.19 Å (HS) and 2.03 Å (LS), for Fe1 and Fe2, respectively.

In turn, the lattice of **2** contains one $(SiF_6$@[Fe(L1)(L3)$_2$]$)^{2+}$ unit (Fig. S4) and two PF_6^- anions crystallographically independent (plus solvents). The supramolecular assembly in **2** is analogous to that of **1**, with a core almost identical; the Fe(II) atoms separated 10.172 Å and a Fe–Si–Fe angle of 153.04°. The effects of the methyl substituents of L3 lead here to a marked difference between the magnetic states of both Fe centers. Thus, at 100K, the Fe–N bond distances average 2.17 and 2.04 Å for Fe1 and Fe2, respectively, demonstrating that they are fully in the HS and LS state. The structure of **2a** (Fig. S5) is very similar to that of **2**, with BF_4^- counter-ions instead of PF_6^- (see all structural details in the SI). In contrast to the other three derivatives, both Fe centers of **2a** are found clearly to be fully in the HS state at 100K (average Fe–N distances of 2.20 and 2.18 Å for Fe1 and Fe2, respectively). This difference is also mirrored by the bulk magnetic properties (see below).

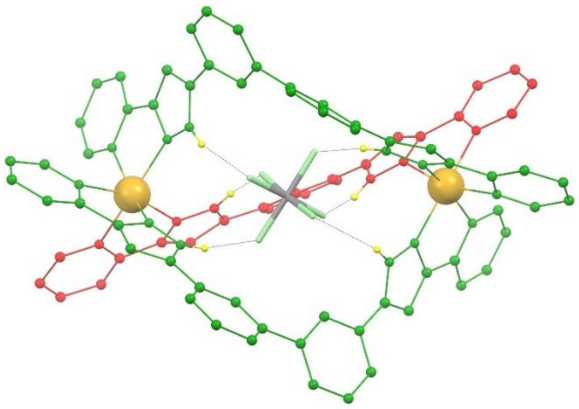

Figure 2. Representation of the supramolecular assembly SiF_6@[Fe_2(L1)(L2)$_2$]$^+$ of **1**. Large yellow balls are Fe(II), small yellow balls are H from N–H groups (rest of hydrogen not shown), red balls are atoms from L1, green balls are atoms from L2, central moiety in stick style is SiF_6^{2-}, hydrogen bonds are shown as black, dashed lines.

Heteroleptic $[M_xL_yL'_z]^m$ metallohelicates have virtually no precedent. A related example is a double heterostranded system of two $[Re(CO)_3]^+$ centres connected by one bis-monodentate and one bis-chelating ligand, capitalizing on the favourable combination of donors to saturate the vacant coordination sites of Re(I).[38] The system reported here is thus the first one where the template effect of a guest drives the assembly of a heteroleptic helicate.

The template effect by SiF_6^{-2} is corroborated by the fact that no helicate with this guest can be isolated with neither of both types of ligands. This exclusive formation of the mixed-ligand construct is in contrast to that of the homoleptic counterparts, $(X$@[Fe_2(L1)$_3$]$)^{3+}$ (X= Cl^-, Br^-)[32] and $(ClO_4$@[Fe_2(L')$_3$]$)^{3+}$ (L' = L2, **3**; L3, **4**, see below) accomodating a small and a large guest, respectively. While ClO_4^- is not bigger than SiF_6^{2-}, it does not have the symmetry to template the formation of the mixed ligand system. The persistence of the $(SiF_6$@[Fe(L1)(L')$_2$]$)^{2+}$ architectures in solution was assessed by ^{19}F NMR on compound **2a**. The spectrum in MeCN (S6) furnishes signals for BF_4^- and SiF_6^{2-} that approximately integrate for the expected 2:1 concentration ratio (4:3 ratio in F) and are attributed to the free ions and guest species, respectively. Indeed, the latter signal shows a much larger broadening than the other, caused by the proximity of the paramagnetic Fe(II) centers. A small signal with intensity one order of magnitude smaller is attributed to an impurity of free SiF_6^{2-}. This was corroborated by the subsequent addition of SiF_6^{2-} (in form of its Bu_4N^+ salt) to the tube, increasing the intensity of this signal without modifying the intensity ratio of the other two peaks (Fig. S6).

An intriguing observation is the drive for SiF_6^{2-} encapsulation in contrast to PF_6^-, which was never found in the cavity. This differential selectivity was quantified through DFT calculations. The calculated energy associated to the process in eq. 2, after geometry optimization and including the influence of the solvent (MeOH and MeCN) was −38 kcalmol^{-1} for both, L' = L2 and L3 (see SI for details).

$$(PF_6$@[Fe(L1)(L')$_2$]$)^{3+} + SiF_6^{2-} \rightarrow (SiF_6$@[Fe(L1)(L')$_2$]$)^{2+} + PF_6^- \quad (2)$$

The remarkable energy advantage of encapsulated SiF_6^{2-} wrt PF_6^- is attributed to much more efficient [E–F···H–N] hydrogen bonds for E=Si than for E=P and/or to the much higher affinity for a guest with two negative charges rather than only one, by a host with charge +4.

The reactions of $Fe(ClO_4)_2$ with L2 or L3 in MeOH produce, respectively, the complex salts ClO_4@[Fe_2(L2)$_3$]$(ClO_4)_3$ (**3**) and ClO_4@[Fe_2(L3)$_3$]$(ClO_4)_3$ (**4**), made by homoleptic helicates.

The asymmetric unit of **3**, obtained from recrystallization in MeCN, includes the host-guest assembly $(ClO_4$@[Fe_2(L2)$_3$]$)^{3+}$, three ClO_4^- anions, four defined solvent molecules and additional diffuse solvent (details in the SI). The unit $(ClO_4$@[Fe_2(L2)$_3$]$)^{3+}$ (Fig. 3 and S7) is a homoleptic helicate made of three bis-pyrazolylpyridine L2 ligands that chelate two Fe(II) centers (separated by 11.018 Å) encapsulating a ClO_4^- guest. The geometrical mismatch between the guest and the host breaks the idealized binary symmetry of the assembly (*eg.* the Fe···Cl separations are 6.075 and 4.983 Å) yielding an array

of [Cl–O···H–N] hydrogen bonds of diverse strengths (Fig. 3 and S7, caption, Table S3).

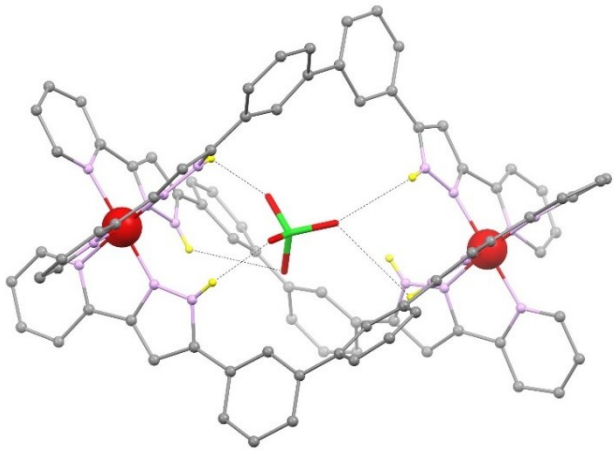

Figure 3. Representation of the supramolecular assembly ClO_4@$[Fe_2(L2)_3])^{3+}$ of **3**. Large red balls are Fe(II), small yellow balls are H from N–H groups (rest of hydrogen not shown), grey balls are C, central moiety in stick style is ClO_4^-, hydrogen bonds are shown as black dashed lines.

The average Fe–N bond distances of the pseudo-octahedral Fe(II) centers are 1.970 and 1.972 Å for Fe1 and Fe2, respectively, showing that both centers lye in the LS state (at 100K, temperature of the data collection), in sharp contrast with the heteroleptic counterparts.

Compound **4** is the analogue of **3** with ligand L3. The lattice contains one $(ClO_4$@$[Fe_2(L3)_3])^{3+}$ unit (Fig. S8), three ClO_4^- anions, and solvent molecules. The main structural parameters of **3** are reproduced in **4** (see SI) with Fe···Fe and Fe···Cl separations of 11.531, 6.698 (Fe1) and 4.839 (Fe2) Å, respectively, and average Fe–N distances of x.xxx (Fe1) and x.xxx (Fe2), thus, also showing LS centers.

The diversity in solid-state magnetic properties of compounds **1** to **4** inferred by their structural parameters was corroborated through variable temperature magnetic susceptibility measurements, carried out under a constant magnetic field of 0.5 T. The χT *vs* T plots (Fig. 4) show that the Fe(II) centers in all cases are spin active.

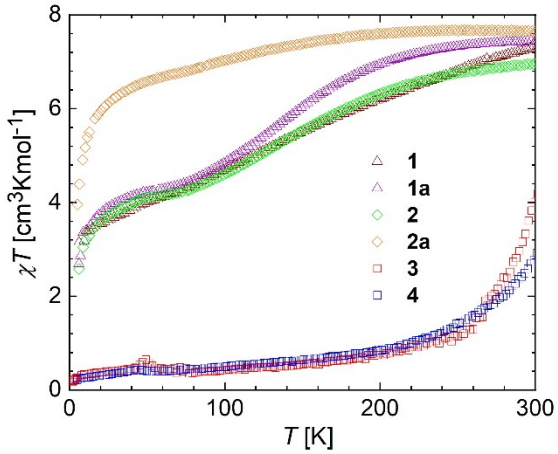

Figure 4. Plots of $\chi_M T$ *vs* T for compounds **1**, **1a**, **2**, **2a**, **3** and **4** (see legend). The measurements were collected on freshly prepared crystals that never reached temperatures above 300 K.

Compounds **1**, **1a**, **2** and **2a** exhibit a sharp increase of χT with T at very low temperature, caused by HS Fe(II) centers not following the Curie Law in this range. This sharp increase attenuates rapidly in the 10 – 20 K range to values of 3 to 3.5 cm^3Kmol^{-1} for **1**, **1a** and **2**, and around 6 cm^3Kmol^{-1} for **2a**. This shows that the first group of compounds exhibit one Fe in the HS and the other in LS, whereas the Fe ions of **2a** are all HS (as suggested by the SCXRD data at 100 K, see above). The mixed-spin compounds exhibit a pseudo plateau suggesting the persistence of approximately 50% of Fe centers in either the HS or the LS state up to around 70 K. Further warming causes a gradual increase of the χT *vs* T curve indicating a broad conversion to the HS state of the *ca.* one half of the metal centers that were in the LS state. Compound **2a**, shows upon warming only a slight and broad increase of χT up to 7.6 cm^3Kmol^{-1} at 300K, suggesting that a very small fraction of Fe(II) being in the LS state at low temperatures experience a very gradual transition to the HS state. Compounds **3** and **4** are almost diamagnetic over most of the temperature range examined, therefore they contain only LS Fe(II) centers. In both cases, the gradual raise of χT *vs* T occurring especially beyond 250 K, denotes a slow conversion to the HS state of these centers that is far from completion at 300 K (approximately 40 to 50%). All these data correspond to samples never been warmed beyond 300 K. Below this temperature, the magnetic response remains fully reversible with temperature. Beyond room temperature the data were not analyzed since they exhibit irreversible changes that are caused most likely by the desorption of lattice solvent molecules, leading expectedly to changes to the SCO behavior.[32]

In summary, this report demonstrates that within the cavity of coordination metallohelicates, the presence of H-bonding groups can be exploited to drive the quantitative formation of heteroleptic assemblies *via* a template effect. This can be exploited to introduce combinations of functions or properties within the assembly thanks to the ability of incorporating different ligands into the architecture. To generalize this methodology, the preparation of analogues of different divalent metals is now under investigation.

This research was supported by Spanish MINECO (PGC2018-098630-B-I00, MAT2017-86826-R), the Aragón government (E31_20R PLATON), the EU (FET-OPEN grant 862893 FATMOLS) and the IN2UB (Masters Fellowship to NC), and used resources of the ALBA synchrotron and of the Advanced Light Source, which is a DOE Office of Science User Facility under contract no. DEAC02-05CH11231. G. A. thanks the Generalitat de Catalunya for the prize ICREA Academia 2018.

Conflicts of interest

There are no conflicts to declare.

Notes and references

‡

1. C. Piguet, G. Bernardinelli and G. Hopfgartner, *Chem. Rev.* 1997, **97**, 2005-2062.
2. M. Albrecht, *Chem. Rev.* 2001, **101**, 3457-3498.
3. M. Elhabiri and A. M. Albrecht-Gary, *Coord. Chem. Rev.* 2008, **252**, 1079-1092.
4. J. M. Lehn, A. Rigault, J. Siegel, J. Harrowfield, B. Chevrier and D. Moras, *Proceedings of the National Academy of Sciences* 1987, **84**, 2565-2569.
5. J. M. Lehn, *Proceedings of the National Academy of Sciences* 2002, **99**, 4763-4768.

6. F. Zou, X. Tang, Y. Huang, S. Wan, F. Lu, Z.-N. Chen, A. Wu and H. Zhang, *CrystEngComm* 2016, **18**, 6624-6631.
7. L. Li, A. R. Craze, R. Akiyoshi, A. Tsukiashi, S. Hayami, O. Mustonen, M. M. Bhadbhade, S. Bhattacharyya, C. E. Marjo, Y. Wang, L. F. Lindoy, J. R. Aldrich-Wright and F. Li, *Dalton Trans.* 2018, **47**, 2543-2548.
8. V. A. Grillo, E. J. Seddon, C. M. Grant, G. Aromí, J. C. Bollinger, K. Folting and G. Christou, *Chem. Commun.* 1997, **1997**, 1561-1562.
9. C.-S. Tsang, L. Chen, L.-W. Li, S.-M. Yiu, T.-C. Lau and H.-L. Kwong, *Dalton Trans.* 2015, **44**, 13087-13092.
10. L. Aboshyan-Sorgho, M. Cantuel, G. Bernardinelli and C. Piguet, *Dalton Trans.* 2012, **41**, 7218.
11. C.-S. Tsang, H.-L. Yeung, W.-T. Wong and H.-L. Kwong, *Chem. Commun.* 2009, DOI: 10.1039/b900264b, 1999.
12. S. Bullock, L. J. Gillie, L. P. Harding, C. R. Rice, T. Riis-Johannessen and M. Whitehead, *Chem. Commun.* 2009, DOI: 10.1039/b908911j, 4856.
13. M. T. Youinou, R. Ziessel and J. M. Lehn, *Inorg. Chem.* 1991, **30**, 2144-2148.
14. M. Albrecht, *Eur. J. Inorg. Chem.* 2020, **2020**, 2227-2237.
15. F. Habib, J. Long, P.-H. Lin, I. Korobkov, L. Ungur, W. Wernsdorfer, L. F. Chibotaru and M. Murugesu, *Chem. Sci.* 2012, **3**, 2158.
16. Y. Li, Y. Zhou, Y. Yao, T. Gao, P. Yan and H. Li, *New J. Chem.* 2021, **45**, 7196-7203.
17. G. Aromí, H. Stoeckli-Evans, S. J. Teat, J. Cano and J. Ribas, *J. Mater. Chem.* 2006, **16**, 2635-2644.
18. S. Floquet, M. Borkovec, G. Bernardinelli, A. Pinto, L.-A. Leuthold, G. Hopfgartner, D. Imbert, J.-C. G. Bünzli and C. Piguet, *Chem., Eur. J.* 2004, **10**, 1091-1105.
19. Y. Furusho, H. Goto, K. Itomi, H. Katagiri, T. Miyagawa and E. Yashima, *Chem. Commun.* 2011, **47**, 9795.
20. M. Albrecht, O. Blau and J. Zauner, *Eur. J. Org. Chem.* 1999, **1999**, 3165-3169.
21. R. W. Saalfrank, H. Maid, N. Mooren and F. Hampel, *Angew. Chem., Int. Ed.* 2002, **41**, 304-307.
22. X.-H. Fu, W.-Y. Wu, P. Jiang, Z.-Y. Han and R. Wan, *Quimica Nova* 2018, **41**, 528-532.
23. P. J. Steel and D. A. McMorran, *Chemistry – An Asian Journal* 2019, **14**, 1098-1101.
24. R. Vilar, *Angew. Chem., Int. Ed.* 2003, **42**, 1460-1477.
25. R. Diego, A. Pavlov, M. Darawsheh, D. Aleshin, J. Nehrkorn, Y. Nelyubina, O. Roubeau, V. Novikov and G. Aromí, *Inorg. Chem.* 2019, **58**, 9562-9566.
26. D. Pelleteret, R. Clerac, C. Mathoniere, E. Harte, W. Schmitt and P. E. Kruger, *Chem. Commun.* 2009, DOI: 10.1039/B816196H, 221-223.
27. H. Hagiwara, T. Tanaka and S. Hora, *Dalton Trans.* 2016, **45**, 17132-17140.
28. L. Zhang, H. Li, P. Chen, W. Sun and P. Yan, *Chem. Res. Chin. Univ.* 2016, **32**, 534-538.
29. J. Zhang, Y. Zhou, Y. Yao, Z. Cheng, T. Gao, H. Li and P. Yan, *J. Mater. Chem., C* 2020, **8**, 6788-6796.
30. A. M. Castilla, T. K. Ronson and J. R. Nitschke, *J. Am. Chem. Soc.* 2016, **138**, 2342-2351.
31. M. Estrader, J. Salinas Uber, L. A. Barrios, J. Garcia, P. Lloyd-Williams, O. Roubeau, S. J. Teat and G. Aromí, *Angew. Chem., Int. Ed.* 2017, **56**, 15622-15627.
32. M. Darawsheh, L. A. Barrios, O. Roubeau, S. J. Teat and G. Aromí, *Chem., Eur. J.* 2016, **22**, 8635-8645.
33. D. Y. Aleshin, R. Diego, L. A. Barrios, Y. V. Nelyubina, G. Aromí and V. V. Novikov, *Angew. Chem., Int. Ed.* 2022, **61**, e202110310.
34. M. Darawsheh, L. A. Barrios, O. Roubeau, S. J. Teat and G. Aromí, *Angew. Chem., Int. Ed.* 2018, **57**, 13509-13513.
35. J. Lee, S. Park, D. Kim, Y.-A. Lee and O.-S. Jung, *Inorg. Chem. Front.* 2020, **7**, 1546-1552.
36. G. A. Van Albada, O. Roubeau, I. Mutikainen, U. Turpeinen and J. Reedijk, *New J. Chem.* 2003, **27**, 1693-1697.
37. H. Casellas, A. Pevec, B. Kozlevčar, P. Gamez and J. Reedijk, *Polyhedron* 2005, **24**, 1549-1554.
38. B. Shankar, S. Sahu, N. Deibel, D. Schweinfurth, B. Sarkar, P. Elumalai, D. Gupta, F. Hussain, G. Krishnamoorthy and M. Sathiyendiran, *Inorg. Chem.* 2014, **53**, 922-930.